Soft Matter

Accepted Manuscript

This article can be cited before page numbers have been issued, to do this please use: L. Hu, H. Zhou, H. Zhu, T. Fan and D. Zhang, *Soft Matter*, 2014, DOI: 10.1039/C4SM01413H.

ROYAL SOCIETY OF CHEMISTRY

www.rsc.org/softmatter

View Article Online
DOI: 10.1039/C4SM01413H

Graphical abstract

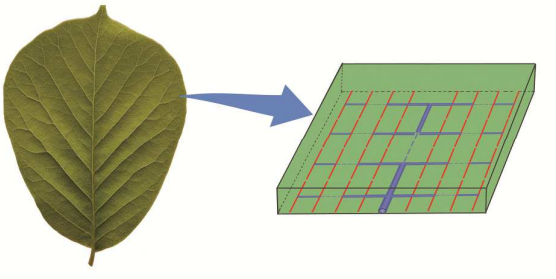

The pinnate leaf architecture, a pervasive natural network-matrix architecture endowing the pinnate leaf with high transpiration rate and low water pressure drop, inspires efficient network-matrix architecture for general flow transport.

ARTICLE TYPE
www. rsc.org/xxxxxx | XXXXXXXX

Efficient network-matrix architecture for general flow transport inspired by natural pinnate leaves†

View Article Online
DOI: 10.1039/C4SM01413H

Liguo Hu,[a] Han Zhou,[a] Hanxing Zhu,[b] Tongxiang Fan,*[a] and Di Zhang[a]

Received Xth XXXXXXXXXX 20XX, Accepted Xth XXXXXXXXX 20XX
First published on the web Xth XXXXXXXXXX 200X
DOI: 10.1039/b000000x

Networks embedded in three dimensional matrices are beneficial to delivering physical flows to the matrices. Leaf architectures, pervasive natural network-matrix architectures, endow leaves with high transpiration rates and low water pressure drops, providing inspiration for efficient network-matrix architectures. In this study, the network-matrix model for general flow transport inspired by natural pinnate leaves is investigated analytically. The results indicate that the optimal network structure inspired by natural pinnate leaves can greatly reduce the maximum potential drop and the total potential drop caused by the flow through the network while maximizing the total flow rate through the matrix. These results can be used to design efficient networks in network-matrix architectures for a variety of practical applications, such as tissue engineering, cell culture, photovoltaic devices and heat transfer.

1 Introduction

Network-matrix architectures have drawn considerable attention and have been applied to a variety of practical applications, such as tissue engineering [1–3], cell culture [4], photovoltaic devices [5] and heat transfer [6] recently. The networks serve as the pathways to deliver (or extract) physical flows (*e.g.*, nutrient flows, electrolyte flows and heat flow) to (or from) the matrices. The total flow rates through the matrices and the potential drops (*i.e.*, the maximum potential drop and the total potential drop) caused by the flows are the most important parameters for measuring the performance of the network-matrix architectures. Few studies have been conducted to investigate the efficiency of the networks in such network-matrix architectures, although great efforts have been made to discover the most efficient transport network which minimizes the total energy dissipation rate [7–11]. Networks in nature are usually embedded in three dimensional matrices, composing natural network-matrix architectures, such as the vascular systems of plants and animals. The plant leaf is a pervasive example of natural network-matrix architectures, inspiring us with an efficient network in the network-matrix architecture which can greatly reduce the potential drops (*i.e.*, the maximum potential drop and the total potential drop) caused by the flow while maximizing the total flow rate through the matrix.

Photosynthesis, the desideratum of living plant leaves, is closely coupled with the total water flow rate through leaves because of the shared diffusional pathway for carbon dioxide and water vapor [12,13]. In fact, the maximum photosynthesis rates of leaves scale linearly with their water transport capacity [13–15]. However, leaf mesophyll is specialized for photosynthesis and imposes a high level of resistance upon the water flowing through it [16]. Moreover, water in plant leaves is pulled forward by negative pressure (tension) created by transpiration [17,18], and water is in a thermodynamically metastable state with respect to vapor phase under negative pressure [19]. When water potential is lower than cavitation threshold pressure, cavitation in water will occur, which disrupts water supply and then limits photosynthesis of leaves [20,21]. Thus, leaves evolve vein networks to maximize the water flow rate through leaves [13,16] and minimize water pressure drops caused by the water flow [20,22]. The terminology for describing leaf vein networks has been summarized by Hickey [23]. In general, the first-order veins are the thickest veins originating at the base of the plant blade, with the second-order veins branching off at intervals, the third-order veins mainly branching off from the second-order veins, *etc.*, as shown in figure 1(a). We consider plant leaves to be optimal architectures for water flow transport selected by nature during a long evolutionary period, which can properly meet the primary physiological functions of maximizing the water flow rate through leaves and minimizing the water pressure drops caused by the water flow.

In this study, we focus on the question whether plant leaf-like architecture is an efficient network-matrix architecture for general flow transport, which can minimize the potential drops (*i.e.*, the maximum potential drop and the total potential drop) caused by the flow while maximizing the total flow rate

† Electronic Supplementary Information (ESI) available: [Video of water flow in Magnolia denudata leaf]. See DOI: 10.1039/b000000x/

[a] *State Key Lab of Composites, Shanghai Jiaotong University, Shanghai, P. R.China. Fax: +86-21-34202749; Tel: +86-21-54747779; E-mail: txfan@sjtu.edu.cn*
[b] *School of Engineering, Cardiff University, Cardiff, UK*

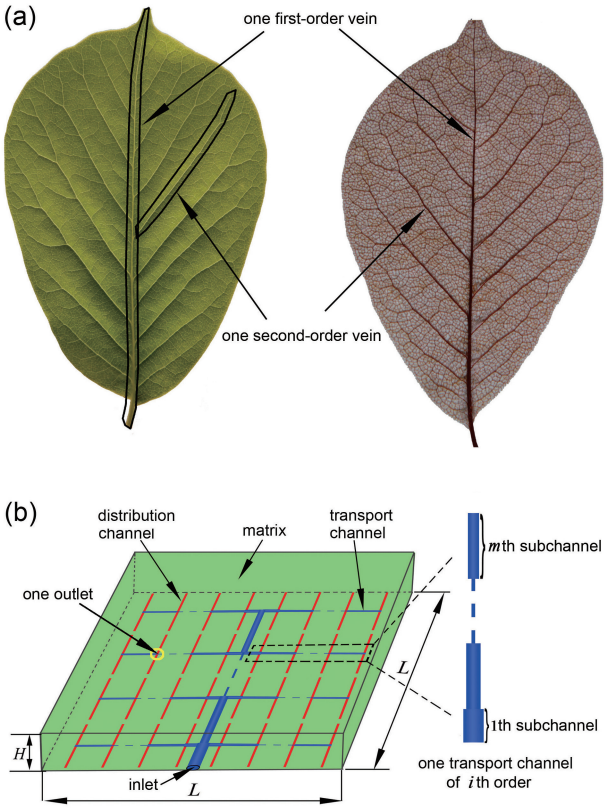

Fig. 1 (a) Picture and vein network of a pinnate leaf (Magnolia denudata leaf); (b) Schematic of the pinnate leaf-like model.

through the matrix. Plant leaves are diverse in their morphology and can be classified as pinnate leaves, palmate leaves and parallel leaves based on leaf vein network structures[24]. The pinnate leaf vein network is hierarchical and one vein of each order, especially the vein of low order (large vein), is tapered with several higher-order veins branching off from it (see figure 1(a)), characterizing the common features of all the three types of leaf vein networks[23,25]. The pinnate leaf vein network can be considered as a general fractal-like network different from the fractal-like networks in previous references[26–29], that is, one vein of each order, especially the vein of low order (large vein), can be treated as several subveins with different diameters rather than a uniform one. Herein, the network-matrix architecture inspired by the pinnate leaf is investigated analytically and the results indicate that the optimal network can greatly reduce the maximum potential drop and the total potential drop caused by the flow transporting through the network while maximizing the total flow rate through the matrix. These results can be used to design efficient networks in network-matrix architectures for a variety of practical applications.

2 Pinnate leaf-like model

View Article Online
DOI: 10.1039/C4SM01413H

Inspired by natural pinnate leaves, we propose a pinnate leaf-like model. In this model, a pinnate leaf-like high conductivity material network, which is equivalent to vein networks in pinnate leaves, is embedded in a low conductivity material matrix, which is equivalent to leaf mesophyll, as shown in figure 1(b). In pinnate leaves, water enters leaves from the petiole, flows from the first-order vein to the second-order veins, then to the third-order veins, and finally to the minor veins, from which water is transmitted to leaf mesophyll (video is available in supplemental material). In short, large veins are used to transport water and minor veins act as a distribution system that delivers water to leaf mesophyll[30,31]. Thus, the high conductivity material network in the pinnate leaf-like model is assumed to consist of transport channels (blue channels in figure 1(b)), which are equivalent to large veins in pinnate leaves, and distribution channels (red channels in figure 1(b)), which are equivalent to minor veins in pinnate leaves. Taking a close look at the pinnate leaf vein network (figure 1(a)), it can be found that one vein of each order, especially the vein of low order (large vein), has a tapered and non-uniform cross section. The vein diameter reduces along the length of a vein, especially where there is a higher order vein branching off from it[32]. One transport channel of each order in the pinnate leaf-like model is thus assumed to consist of several subchannels with different diameters, and for simplicity, the transport channels are considered to be self-similar.

Figure 1(b) shows the detailed description of the pinnate leaf-like model. The size of the square matrix with uniform thickness is $L\times L\times H$. The network consists of transport channels (blue channels) and distribution channels (red channels). One transport channel of each order consists of m ($m \geq 1$) subchannels, and the total number of orders of the transport channels is n. The total length of an ith order transport channel is L_i and the length of the jth subchannel of an ith order transport channel is l_{ij}. The diameter of the jth subchannel of an ith order transport channel is d_{ij}. The distance between the neighboring distribution channels is d and the length of distribution channels is L_d. Given the uniform distribution of the identical distribution channels, one obtains

$$l_{i1} : l_{i2} : \ldots : l_{im} = 1 : 2 : \ldots : 2. \quad (1)$$

From figure 1(b), one can also easily have

$$L_i = \begin{cases} \dfrac{2m-1}{2m}\left(\dfrac{1}{2m}\right)^{\frac{i-1}{2}} L & i = \text{odd number} \\ \dfrac{2m-1}{2m}\left(\dfrac{1}{2m}\right)^{\frac{i-2}{2}} \dfrac{L}{2} & i = \text{even number} \end{cases}, \quad (2)$$

$$L_d = \begin{cases} \left(\frac{1}{2m}\right)^{\frac{n-1}{2}} \frac{L}{2} & n = \text{odd number} \\ \left(\frac{1}{2m}\right)^{\frac{n}{2}} L & n = \text{even number} \end{cases}, \quad (3)$$

$$d = \begin{cases} \left(\frac{1}{2m}\right)^{\frac{n-1}{2}} \frac{L}{m} & n = \text{odd number} \\ \left(\frac{1}{2m}\right)^{\frac{n}{2}} L & n = \text{even number} \end{cases}. \quad (4)$$

The total number of the ith order transport channels N_i can be obtained as

$$N_i = (2m)^{i-1}. \quad (5)$$

3 Results

3.1 Optimal distance between distribution channels

Total water flow rate through a leaf is determined by the distance between the neighboring minor veins (or minor vein density)[16,33]. Noblin *et al.*[34] have analytically demonstrated that the optimal distance between the neighboring minor veins, which maximizes the total water flow rate, is proportional to thickness of leaves. Following the analytical calculation of Noblin *et al.*, we can extend the result from water flow in leaves to general flow (*e.g.*, nutrient flows, electrolyte flows and heat flow) in the pinnate leaf-like model. The optimal distance between neighboring distribution channels, which maximizes the total flow rate through the matrix, is proportional to the thickness of the pinnate leaf-like model and expressed as

$$d_{opt} = \chi H. \quad (6)$$

Where d_{opt} is the optimal distance between the neighboring distribution channels maximizing the total flow rate through the matrix, and χ is the proportionality factor[34]. Equation 6 is the foundation of optimizing the transport channel system (*i.e.*, different structures of the transport channel system should maintain the optimal distance between the neighboring distribution channels).

3.2 Optimal pinnate leaf-like transport channel system

In the following, we optimize the transport channel (blue channels in figure 1(b)) system, which connects the distribution channels with the optimal distance maximizing the total flow rate through the matrix, to minimize the maximum potential drop caused by the flow transporting through the transport channel system. The pinnate leaf-like transport channel system presented in this study can be considered as a general fractal-like structure, that is, one transport channel of each order consists of m ($m \geq 1$) subchannels rather than one uniform channel in the fractal-like structures in previous references[26–29]. Comparing equations 3 and 4, it can be obtained that $L_d = md/2$ if n is an odd number and $L_d = d$ if n is an even number. Because the optimal distance between the neighboring distribution channels is a constant (*i.e.*, $d_{opt} = \chi H$), the length of the distribution channels remains unchanged with the variation of m if n is an even number. In the following calculation, n is assumed to be an even number, so that for different transport channel system structures (different values of m) we can obtain the same distribution of distribution channels (same length of the distribution channels and same distance between the neighboring distribution channels). The maximum potential drop $\Delta\psi_{max}$ through the transport channel system is calculated as

$$\Delta\psi_{max} = \sum_{i=1}^{n} \sum_{j=1}^{m} \Delta\psi_{ij}. \quad (7)$$

Where $\Delta\psi_{ij}$ is the potential drop along the jth subchannel of an ith order transport channel and defined as[8,35]

$$\Delta\psi_{ij} = \frac{\varepsilon l_{ij} q_{ij}}{d_{ij}^{\alpha}}, \quad (8)$$

where α is a constant characterizing the flow profile (*e.g.*, $\alpha = 2$ indicates that the flow is plug-like, and $\alpha = 4$ indicates that the flow is Poiseuille-like), ε is the "resistivity" of the transport channels, q_{ij} is the flow rate through the jth subchannel of an ith order transport channel. We minimize the maximum potential drop under the global constraint[8,35]

$$\sum_{i=1}^{n} (2m)^{i-1} \sum_{j=1}^{m} \eta d_{ij}^{\beta} l_{ij} = C, \quad (9)$$

where C is a constant and can be interpreted as the amount of high conductivity material available to build the transport channel system, β is a parameter characterizing the constraint (*e.g.*, $\beta = 1$ indicates constant total surface constraint, and $\beta = 2$ indicates constant total volume constraint) and η is a coefficient that depends on specific constraints (*e.g.*, for a constant total surface constraint $\eta = \pi$, for constant total volume constraint $\eta = \pi/4$). In order to minimize $\Delta\psi_{max}$ with the constraint of equation 9, the Lagrange multiplier technique is employed, and one has

$$q_{ij} = \gamma (2m)^{i-1} d_{ij}^{\alpha+\beta}. \quad (10)$$

Where $\gamma = (\lambda\eta\beta)/(\varepsilon\alpha)$ and λ is the Lagrange multiplier. Combining equations 7-10, $\Delta\psi_{max}$ is calculated as

$$\Delta\psi_{max} = \lambda \frac{\beta}{\alpha} C. \quad (11)$$

View Article Online
DOI: 10.1039/C4SM01413H

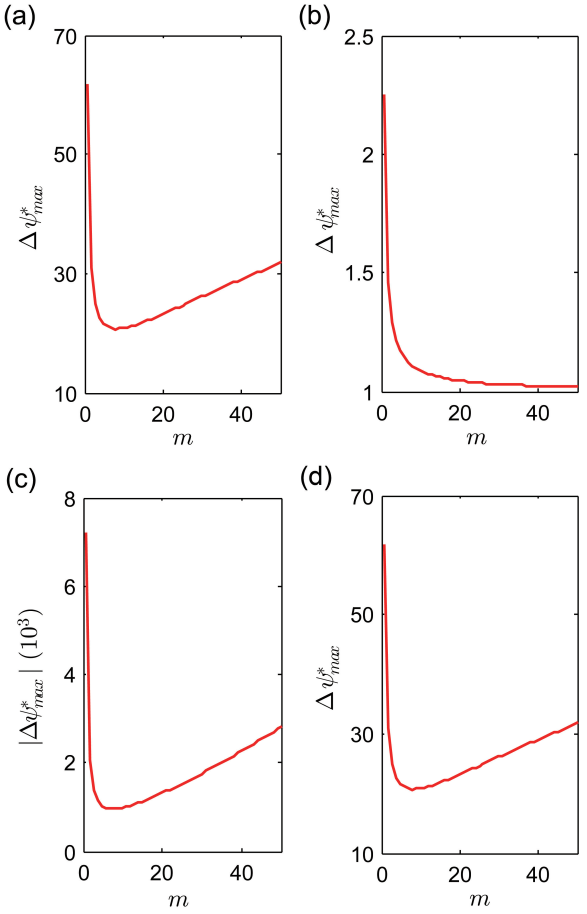

Fig. 2 Relationships between the nondimensional maximum potential drop $\Delta\psi^*_{max}$ and the transport channel system structures determined by the number of subchannels m composing a tapered transport channel (a) Poiseuille-like flow under constant volume constraint; (b) plug-like flow under constant volume constraint; (c) Poiseuille-like flow under constant surface constraint; (d) plug-like flow under constant surface constraint.

The self-similarity and homogeneity of the transport channel system lead to

$$q_{ij} = \left(\frac{m-j+1}{m}\right)\frac{Q}{N_i}. \tag{12}$$

Where Q is total flow rate through the matrix, N_i is the total number of the ith order transport channels. Combining equations 1, 2, 4-6, 9, 10 and 12, one obtains

$$\lambda = \varepsilon Q \frac{\alpha}{\beta}\eta^{\frac{\alpha}{\beta}}\left(\frac{L}{C}\right)^{\frac{\alpha+\beta}{\beta}} f^{\frac{\alpha+\beta}{\beta}}(m)\left(1-\left(\frac{\chi H}{L}\right)^{\frac{3\beta-\alpha}{\alpha+\beta}}\right)^{\frac{\alpha+\beta}{\beta}}. \tag{13}$$

View Article Online
DOI: 10.1039/C4SM01413H

Where $f(m)$ is expressed as

$$f(m) = \left(1+2\sum_{j=2}^{m}\left(\frac{m-j+1}{m}\right)^{\frac{\beta}{\alpha+\beta}}\right) \times \left(\frac{(2m)^{-1}}{1-(2m)^{\frac{\alpha-3\beta}{\alpha+\beta}}} + \frac{1}{2}\frac{(2m)^{\frac{-2\beta}{\alpha+\beta}}}{1-(2m)^{\frac{\alpha-3\beta}{\alpha+\beta}}}\right).$$

Inserting equation 13 into equation 11, one finds

$$\Delta\psi^*_{max} = F(m). \tag{14}$$

Where $\Delta\psi^*_{max} = \Delta\psi_{max}/\delta$ is the nondimensional maximum potential drop, and

$$\delta = \varepsilon Q\left(\frac{\eta}{C}\right)^{\frac{\alpha}{\beta}} L^{\frac{\alpha+\beta}{\beta}}\left(1-\left(\frac{\chi H}{L}\right)^{\frac{3\beta-\alpha}{\alpha+\beta}}\right)^{\frac{\alpha+\beta}{\beta}},$$

$F(m) = [f(m)]^{(\alpha+\beta)/\beta}$. Equation 14 describes the relationship between the pinnate leaf-like transport channel system structures determined by m (the number of subchannels composing a tapered transport channel) and the maximum potential drop evaluated by $\Delta\psi^*_{max}$. The most common flow profiles in nature and in the man-made world are Poiseuille-like (*e.g.*, water flow in plants, blood flow in animals) and plug-like (*e.g.*, heat flow, electrical current), and the most common constraints are constant total volume and constant total surface. Figures 2(a)-2(d) show the cases of Poiseuille-like flow ($\alpha = 4$) under constant volume constraint ($\beta = 2$), plug-like flow ($\alpha = 2$) under constant volume constraint ($\beta = 2$), Poiseuille-like flow ($\alpha = 4$) under constant surface constraint ($\beta = 1$) and plug-like flow ($\alpha = 2$) under constant surface constraint ($\beta = 1$), respectively. As can be seen, the maximum potential drop first decreases dramatically with the increase of m (the number of subchannels composing a tapered transport channel), indicating that the optimal structure of transport channel system can greatly reduce the maximum potential drop.

In addition to the maximum potential drop, the total potential drop (*i.e.*, the flow-rate weighted average potential drop) for the whole transport channel system is another important measure of transport performance. The total potential drop $\overline{\Delta\psi_w}$ is expressed as

$$\overline{\Delta\psi_w} = \sum_{outlets}\omega_k\Delta\psi'_{1k}. \tag{15}$$

Where $\Delta\psi'_{1k}$ is the potential drop between outlet k and inlet 1 of the transport channel system (see figure 1(b)), $\omega_k = q_k/Q$ is the weighted factor of $\Delta\psi'_{1k}$ and q_k is the outflow rate through outlet k. Using equations 8 and 15, one obtains

$$\overline{\Delta\psi_w} = \frac{1}{Q}\sum_{i=1}^{n}(2m)^{i-1}\sum_{j=1}^{m}\frac{\varepsilon l_{ij}q_{ij}^2}{d_{ij}^{\alpha}} = \frac{E}{Q}. \tag{16}$$

Where E is the total energy dissipation rate of the transport channel system, equation 16 means that the total potential drop is proportional to the total energy dissipation rate [36] (that is why we consider the flow-rate weighted average potential drop as the total potential drop). Combining equations 1, 2, 4-6, 10, 12, 13 and 16, it is can be found that $\overline{\Delta\psi_w}$ is also a function of m and given as

$$\overline{\Delta\psi_w}^* = G(m). \tag{17}$$

Where $\overline{\Delta\psi_w}^* = \overline{\Delta\psi_w}/\delta$ is the nondimensional total potential drop, $G(m) = [f(m)]^{\alpha/\beta}\nu(m)$, and $\nu(m)$ is expressed as

$$\nu(m) = \left(1 + 2\sum_{j=2}^{m}\left(\frac{m-j+1}{m}\right)^{\frac{\alpha+2\beta}{\alpha+\beta}}\right) \times \left(\frac{(2m)^{-1}}{1-(2m)^{\frac{\alpha-3\beta}{\alpha+\beta}}} + \frac{1}{2}\frac{(2m)^{\frac{-2\beta}{\alpha+\beta}}}{1-(2m)^{\frac{\alpha-3\beta}{\alpha+\beta}}}\right).$$

Equation 17 describes the effect of the pinnate leaf-like transport channel system structures on the total potential drop. Figures 3(a)-3(d) show the cases of Poiseuille-like flow ($\alpha = 4$) under constant volume constraint ($\beta = 2$), plug-like flow ($\alpha = 2$) under constant volume constraint ($\beta = 2$), Poiseuille-like flow ($\alpha = 4$) under constant surface constraint ($\beta = 1$) and plug-like flow ($\alpha = 2$) under constant surface constraint ($\beta = 1$), respectively. As can be seen, the total potential drop first decreases dramatically with the increase of m (the number of subchannels composing a tapered transport channel), implying that the optimal structure of transport channel system can also greatly reduce the total potential drop.

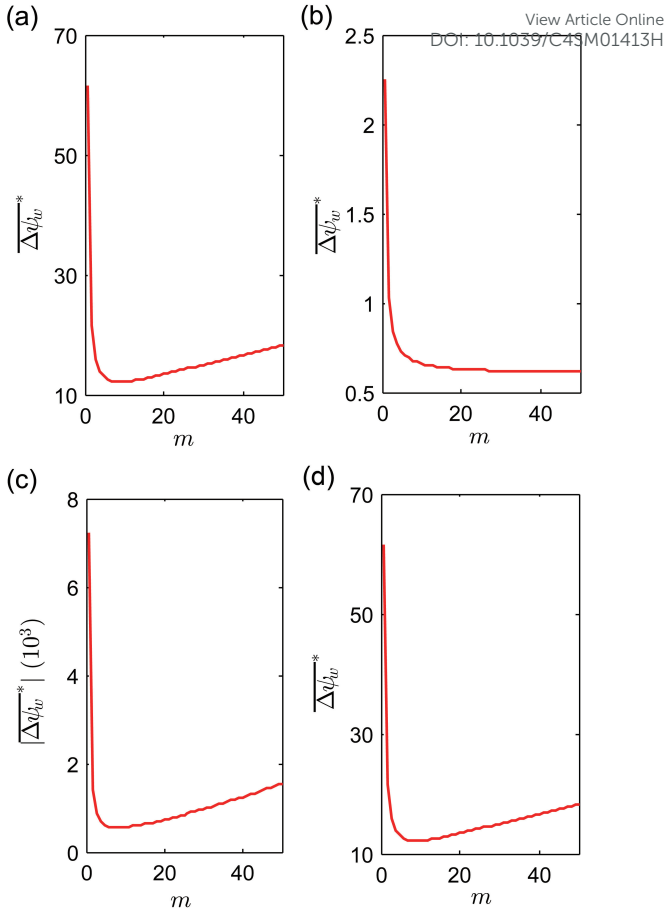

Fig. 3 Relationships between the nondimensional total potential drop $\overline{\Delta\psi_w}^*$ and the transport channel system structures determined by the number of subchannels m composing a tapered transport channel (a) Poiseuille-like flow under constant volume constraint; (b) plug-like flow under constant volume constraint; (c) Poiseuille-like flow under constant surface constraint; (d) plug-like flow under constant surface constraint.

4 Conclusions

Previous studies [7–11,35] have been focused on minimizing the total energy dissipation rate of a network. The networks in many natural and practical applications, however, are embedded in three dimensional matrices, in these cases the total flow rates through matrices and the potential drops caused by the flow through networks are the primary parameters to be optimized. Finding efficient network-matrix architecture for general flow transport is important in practical engineering applications as well as in understanding biophysical physics. In this study, we investigate the network-matrix architecture inspired by the pinnate leaf and analytically demonstrate that the optimal network-matrix architecture inspired by the pinnate leaf is an efficient architecture, which can greatly reduce the maximum potential drop and the total potential drop caused by the flow through the network while maximizing the total flow rate through the matrix. The total flow rate is determined by the distance between the neighboring distribution channels, and there is an optimal distance which maximizes the total flow rate. The maximum potential drop and the total potential drop are determined by transport channel system structures evaluated by a parameter m (the number of subchannels composing a tapered transport channel), and the optimal transport channel system structure can greatly reduce the maximum potential drop and the total potential drop. Techniques of direct ink writing [2,37,38], soft lithography [3,4,39], microreplication [1] and direct laser ablation [40] have been successfully developed to fabricate network-matrix architecture. Using these powerful fabrication technologies, the results obtained in this study can be used to manufacture efficient network-matrix architectures for aforementioned practical applications.

Acknowledgements

We acknowledge the consistent financial supports of National Basic Research Program of China (No. 2012CB619600), the Research Fund for the Doctoral Program of Higher Education (Nos. 20100073110065 and 20110073120036).

Appendix: Constants in the model

Table 1 Summary of constants in the model

constant	physical meaning and/or reference
χ	proportionality factor[34]
α	number characterizing the flow profile[8,35] $\alpha = 2$ indicates plug-like flow $\alpha = 4$ indicates Poiseuille-like flow
ε	"resistivity" of transport channels[8,35]
β	number characterizing the constraint[8,35] $\beta = 1$ indicates total surface constraint $\beta = 2$ indicates total volume constraint
η	coefficient depending on specific constraint for total surface constraint $\eta = \pi$ for total volume constraint $\eta = \pi/4$
C	amount of high conductivity material[8,35]

References

1 J. He, M. Mao, Y. Liu, J. Shao, Z. Jin and D. Li, *Adv. Healthcare Mater.*, 2013, **2**, 1108–1113.
2 J. S. Miller, K. R. Stevens, M. T. Yang, B. M. Baker, D.-H. T. Nguyen, D. M. Cohen, E. Toro, A. A. Chen, P. A. Galie, X. Yu, R. Chaturvedi, S. N. Bhatia and C. S. Chen, *Nat. Mater.*, 2012, **11**, 768–774.
3 M. Cabodi, N. W. Choi, J. P. Gleghorn, C. S. D. Lee, L. J. Bonassar and A. D. Stroock, *J. Am. Chem. Soc.*, 2005, **127**, 13788–13789.
4 Y. Ling, J. Rubin, Y. Deng, C. Huang, U. Demirci, J. M. Karp and A. Khademhosseini, *Lab Chip*, 2007, **7**, 756–762.
5 H.-J. Koo and O. D. Velev, *Sci. Rep.*, 2013, **3**, 2357.
6 A. Mazloomi, F. Sharifi, M. R. Salimpour and A. Moosavi, *Int. Commun. Heat Mass Transf.*, 2012, **39**, 1265–1271.
7 F. Corson, *Phys. Rev. Lett.*, 2010, **104**, 048703.
8 M. Durand, *Phys. Rev. Lett.*, 2007, **98**, 088701.
9 S. Bohn and M. O. Magnasco, *Phys. Rev. Lett.*, 2007, **98**, 088702.
10 J. R. Banavar, F. Colaiori, A. Flammini, A. Maritan and A. Rinaldo, *Phys. Rev. Lett.*, 2000, **84**, 4745–4748.
11 C. D. Murray, *Proc. Natl. Acad. Sci. USA*, 1926, **12**, 207–214.
12 T. J. Brodribb and T. S. Feild, *Ecol. Lett.*, 2010, **13**, 175–183.
13 T. J. Brodribb, T. S. Feild and L. Sack, *Funct. Plant Biol.*, 2010, **37**, 488–498.
14 R. M. Hubbard, M. G. Ryan, V. Stiller and J. S. Sperry, *Plant Cell Environ.*, 2001, **24**, 113–121.
15 T. J. Brodribb, N. M. Holbrook, M. A. Zwieniecki and B. Palma, *New Phytol.*, 2005, **165**, 839–846.
16 C. K. Boyce, T. J. Brodribb, T. S. Feild and M. A. Zwieniecki, *Proc. R. Soc. B-Biol. Sci.*, 2009, **276**, 1771–1776.
17 M. T. Tyree, *J. Exp. Bot.*, 1997, **48**, 1753–1765.
18 T. D. Wheeler and A. D. Stroock, *Nature*, 2008, **455**, 208–212.
19 H. Cochard, *C. R. Phys.*, 2006, **7**, 1018–1026.
20 S. Salleo, A. Nardini, F. Pitt and M. A. LoGullo, *Plant Cell Environ.*, 2000, **23**, 71–79.
21 A. Nardini, M. T. Tyree and S. Salleo, *Plant Physiol.*, 2001, **125**, 1700–1709.
22 A. Roth-Nebelsick, D. Uhl, V. Mosbrugger and H. Kerp, *Ann. Bot.*, 2001, **87**, 553–566.
23 L. J. Hickey, *Am. J. Bot.*, 1973, **60**, 17–33.
24 R. L. Walls, *Am. J. Bot.*, 2011, **98**, 244–253.
25 L. Sack and C. Scoffoni, *New Phytol.*, 2013, **198**, 983–1000.
26 G. B. West, J. H. Brown and B. J. Enquist, *Science*, 1997, **276**, 122–126.
27 G. B. West, J. H. Brown and B. J. Enquist, *Nature*, 1999, **400**, 664–667.
28 P. Xu and B. Yu, *J. Appl. Phys.*, 2006, **100**, 104906.
29 J. Kou, Y. Chen, X. Zhou, H. Lu, F. Wu and J. Fan, *Physica A*, 2014, **393**, 527–534.
30 L. Sack and N. M. Holbrook, *Annu. Rev. Plant Biol.*, 2006, **57**, 361–381.
31 L. Sack, E. M. Dietrich, C. M. Streeter, D. Sánchez-Gómez and N. M. Holbrook, *Proc. Natl. Acad. Sci. USA*, 2008, **105**, 1567–1572.
32 C. A. Price, S.-J. C. Knox and T. J. Brodribb, *PLoS One*, 2013, **8**, e85420.
33 T. J. Brodribb, T. S. Feild and G. J. Jordan, *Plant Physiol.*, 2007, **144**, 1890–1898.
34 X. Noblin, L. Mahadevan, I. A. Coomaraswamy, D. A. Weitz, N. M. Holbrook and M. A. Zwieniecki, *Proc. Natl. Acad. Sci. USA*, 2008, **105**, 9140–9144.
35 M. Durand, *Phys. Rev. E*, 2006, **73**, 016116.
36 E. Katifori, G. J. Szöllősi and M. O. Magnasco, *Phys. Rev. Lett.*, 2010, **104**, 048704.
37 W. Wu, A. DeConinck and J. A. Lewis, *Adv. Mater.*, 2011, **23**, H178–H183.
38 W. Wu, C. J. Hansen, A. M. Aragón, P. H. Geubelle, S. R. White and J. A. Lewis, *Soft Matter*, 2010, **6**, 739–742.
39 L. M. Bellan, T. Kniazeva, E. S. Kim, A. A. Epshteyn, D. M. Cropek, R. Langer and J. T. Borenstein, *Adv. Healthcare Mater.*, 2012, **1**, 164–167.
40 D. Lim, Y. Kamotani, B. Cho, J. Mazumder and S. Takayama, *Lab Chip*, 2003, **3**, 318–323.